Journal of Biomedical Optics

BiomedicalOptics.SPIEDigitalLibrary.org

Digital holographic microscopy for longitudinal volumetric imaging of growth and treatment response in three-dimensional tumor models

Yuyu Li
Ljubica Petrovic
Jeffrey La
Jonathan P. Celli
Chandra S. Yelleswarapu

SPIE.

Digital holographic microscopy for longitudinal volumetric imaging of growth and treatment response in three-dimensional tumor models

Yuyu Li, Ljubica Petrovic, Jeffrey La, Jonathan P. Celli,* and Chandra S. Yelleswarapu*
University of Massachusetts Boston, Department of Physics, 100 Morrissey Boulevard, Boston, Massachusetts 02125, United States

Abstract. We report the use of digital holographic microscopy (DHM) as a viable microscopy approach for quantitative, nondestructive longitudinal imaging of *in vitro* three-dimensional (3-D) tumor models. Following established methods, we prepared 3-D cultures of pancreatic cancer cells in overlay geometry on extracellular matrix beds and obtained digital holograms at multiple time points throughout the duration of growth. The holograms were digitally processed and the unwrapped phase images were obtained to quantify the nodule thickness over time under normal growth and in cultures subject to chemotherapy treatment. In this manner, total nodule volumes are rapidly estimated and demonstrated here to show contrasting time-dependent changes during growth and in response to treatment. This work suggests the utility of DHM to quantify changes in 3-D structure over time and suggests the further development of this approach for time-lapse monitoring of 3-D morphological changes during growth and in response to treatment that would otherwise be impractical to visualize. © *2014 Society of Photo-Optical Instrumentation Engineers (SPIE)* [DOI: 10.1117/1.JBO.19.11.116001]

Keywords: digital holographic microscopy; three-dimensional tumor models; treatment assessment; therapeutic screening; longitudinal imaging; quantitative phase imaging.

Paper 140395PRR received Jun. 22, 2014; revised manuscript received Sep. 23, 2014; accepted for publication Sep. 24, 2014; published online Nov. 3, 2014.

1 Introduction

Conventional optical microscopy techniques such as phase contrast and differential interference contrast are well suited to observe qualitative structural and morphological changes in live cell cultures. However, these ubiquitous contrast enhancement techniques are often inadequate for the study of systems in which the quantitative measurement of three-dimensional (3-D) architecture plays a central role. This need is particularly pronounced in cancer research, where 3-D culture models have become established as powerful tools that restore physiologically-relevant tumor architecture that is lost in traditional monolayer cell culture.[1–10] Although confocal fluorescence microscopy emerges as a natural tool for 3-D optical imaging of these systems, it typically requires staining with fluorophores/conjugates that demand terminal fixation, thereby precluding the possibility of longitudinal imaging of the same specimen. This is a major limitation for studies which seek to explore some of the most provocative features of these cell culture models that require analysis of the dynamic changes in 3-D architecture over time and in response to interventions, in the same specimen. Confocal systems are also costly to purchase and maintain and may not be readily available in all research labs. Hence, there is a need to seek alternate quantitative microscopy techniques that nondestructively provide information on the spatial extent of objects in the z-direction in order to study dynamic changes in 3-D tumor models.

Significant progress has been made in developing new microscopy techniques that are suited for longitudinal monitoring of growth processes in 3-D culture systems.[11–15] For instance digital holographic microscopy (DHM), one of the several types of quantitative phase imaging (QPI) techniques, is a nondestructive, full-field QPI technique that can lay out the structural details in 3-D and is suitable in live cell imaging scenarios.[16–27] DHM is based on the classical holographic principle, with the difference being that the hologram recording is performed by a digital image sensor, e.g., charge-coupled device (CCD) or complementary metal oxide semiconductor (CMOS) sensor array. In DHM, the interference pattern between the object (biological specimen such as cells) and reference beams is recorded using a CCD or a CMOS device. The subsequent reconstruction of the holographic image that contains the information about the object wave is carried out numerically with a computer. In off-axis DHM, the object and reference beams are interfered in the recording media at a certain angle. Hence, a single interferogram is sufficient to reconstruct object information, making this approach ideal for studying dynamic processes in live cells. In-line DHM, as in phase-shifting DHM, the angle between the object and the reference beam is set to zero.[21,28–34] It is worth noting that while other advanced optical imaging techniques have also demonstrated great utility in similar biological models,[35–43] this DHM approach only requires relatively low-cost and widely available optical components.

The present study, leveraging these inherent advantages of DHM for imaging time dependent growth and treatment response processes in 3-D cancer models, is motivated by considerable progress by others in related DHM applications. For example, the DHM systems combined with appropriate custom software for label-free tracking of live cell movements in 3-D environments has been successfully demonstrated by Dubois

*Address all correspondence to: Jonathan P. Celli, E-mail: Jonathan.celli@umb.edu; Chandra S. Yelleswarapu, E-mail: Chandra.yelleswarapu@umb.edu

1083-3668/2014/$25.00 © 2014 SPIE

et al.[44] and Langehanenberg et al.[45] In other studies, the ability of DHM to report the cellular dry mass has been implemented to noninvasively monitor growth processes in live cells,[11,12] and Kuś et al.[46] developed an approach to quantitatively analyze 3-D refractive index distributions from live tumor spheroids. The present work seeks to bring together the progress of the developments in DHM applications referenced above for label-free live cell imaging with the development of 3-D tumor models as a platform for high content therapeutic evaluation.[9,10,47]

Here, we report the use of DHM for nondestructive longitudinal imaging of *in vitro* 3-D tumor nodules formed by an overlay of PANC-1 cells on beds of growth-factor reduced Matrigel. Combined with measurement of the refractive index (n) of 3-D tumor nodules, we converted the optical path length into the physical object height and reliably quantified the tumor volume over time, without making an extensive geometric approximation about the 3-D profile (ellipsoid, spheroid, etc.). To validate this approach, we specifically evaluate changes in 3-D volume under normal growth conditions, and in cultures subject to intervention with oxaliplatin, a platinum-based chemotherapy agent.

2 Materials and Methods

2.1 *Cell Lines and Reagents*

PANC-1 pancreatic cancer cells used in the study were obtained from American Type Culture Collection (ATCC, Rockville, Maryland) and grown according as per ATCC descriptions in media containing 50 IU/mL penicillin and 50-mg/mL streptomycin (Hyclone). Dulbecco's modified Eagle's medium culture media and fetal bovine serum were obtained from Hyclone Laboratories (Logan, Utah). The 3-D cultures of PANC-1 were grown in overlay on a bed of Growth Factor Reduced (GFR) Matrigel™ (BD Biosciences, Bedford, Massachusetts) with media supplemented with 2% GFR Matrigel, adapted from a methodology previously described.[6,48] Cultures were plated in MatTek Glass Bottom Culture Dishes (MatTek Corporation, Ashland, Massachusetts), which enable high quality optical imaging through the dish bottom. Media were changed once every third day during the growth process.

2.2 *Chemotherapy Treatment*

For treatment response, solutions of Oxaliplatin (Selleck Chemicals, Houston, Texas) in 20 and 100-μM concentrations were prepared in the growth medium and added to the cultures at day 3. Cultures were incubated in media containing the chemotherapy agent for 72 h. After 3-days, media was removed and fresh media without chemotherapy was added for further monitoring of the growth process.

2.3 *DHM Image Acquisition and Processing*

The growth rate and treatment response of PANC-1 tumor nodules were imaged using an implementation of a typical off-axis DHM setup, shown in Fig. 1(a). The output of an Ar-Kr laser ($\lambda = 488$ nm) is spatially filtered and well collimated. It is then divided into two beams using a beam splitter—one to transmit through the sample (hence termed as the object beam) and the other to serve as a reference beam. The object beam is coupled into a Zeiss (Jena, Germany) Axiovert 100 Observer A1 inverted microscope. Light transmitted through the sample is collected using a Zeiss EC Epiplan-Neofluar 20× microscope objective and is collected from one of the video ports of the microscope. It is then relayed onto a SPOT Insight™ 2-MP Firewire CCD camera using a long focal length lens. The reference beam is made to interfere with the object beam at the camera with a certain angle between them (off-axis geometry) to create a uniform fringe structure oriented at 45 deg with respect to the x and y axes of the CCD. The white light source of the microscope is used to obtain bright field images. Imaging was performed on the same cultures at discrete time points in between which cell cultures were returned to the CO_2 incubator. Individual culture dishes were on the microscope stage at lab atmosphere for only brief intervals, ~15 min, at each imaging time point.

There were two dishes for each group—no treatment, 20 μM, and 100-μM oxaliplatin treatment. We acquired approximately 10 images per dish at randomly selected sites. As the field-of-view was large, there were about three multicellular nodules per image. Therefore, statistically each group represents the imaging of about 60 nodules per day. All images were processed and organized by timepoint and treatment group to generate analysis of the treatment-dependent growth behavior. Additionally, the entire experiment was rerun three times with a minimal variation of treatment timepoints and other parameters with almost identical results.

Reconstruction of the digitally recorded holograms is numerically performed by a standard computer. A detailed phase reconstruction of the object wave procedure is described elsewhere.[18,19,49,50] In short, the digital hologram is Fourier transformed, high pass filtered to eliminate the dc, and the twin image is suppressed. It is then inverse Fourier transformed and unwrapped to obtain the true phase information of the object. In order to obtain 3-D morphological parameters, the phase map $\phi(x, y)$ is converted to a height map $h(x, y)$ as

$$h(x, y) = \frac{\lambda \phi(x, y)}{2\pi(n_1 - n_2)}, \tag{1}$$

where λ is the wavelength of the light source, n_1 is the refractive index of the specimen and n_2 is the refractive index of the medium.

2.4 *Measurement of Refractive Index of 3-D Tumor Nodules*

A side by side comparison of DHM phase unwrapping and confocal fluorescence z-stacks of the same microscope fields was made to obtain the refractive index of the PANC1 3-D cultures. First, DHM images were obtained and the orientation of the nodules was marked. Cultures were then stained with calcein acetoxymethylesther (calcein AM, BD Biosciences), a fluorescent label for viable cells, and placed on the confocal microscope stage in precisely the same orientation so that exactly the same nodules could be imaged. In this manner, the optical path length obtained by DHM, combined with the coregistered physical object height from confocal imaging, is used to solve using Eq. (1) for the refractive index for individual nodules (relative to the known index of the surrounding medium) and calculated a mean value.

2.5 *Fluorescence Imaging and Analysis*

DHM quantification of the treatment response was also validated by an established method based on the quantification of the signal from the fluorescent reporters of cell viability,[9]

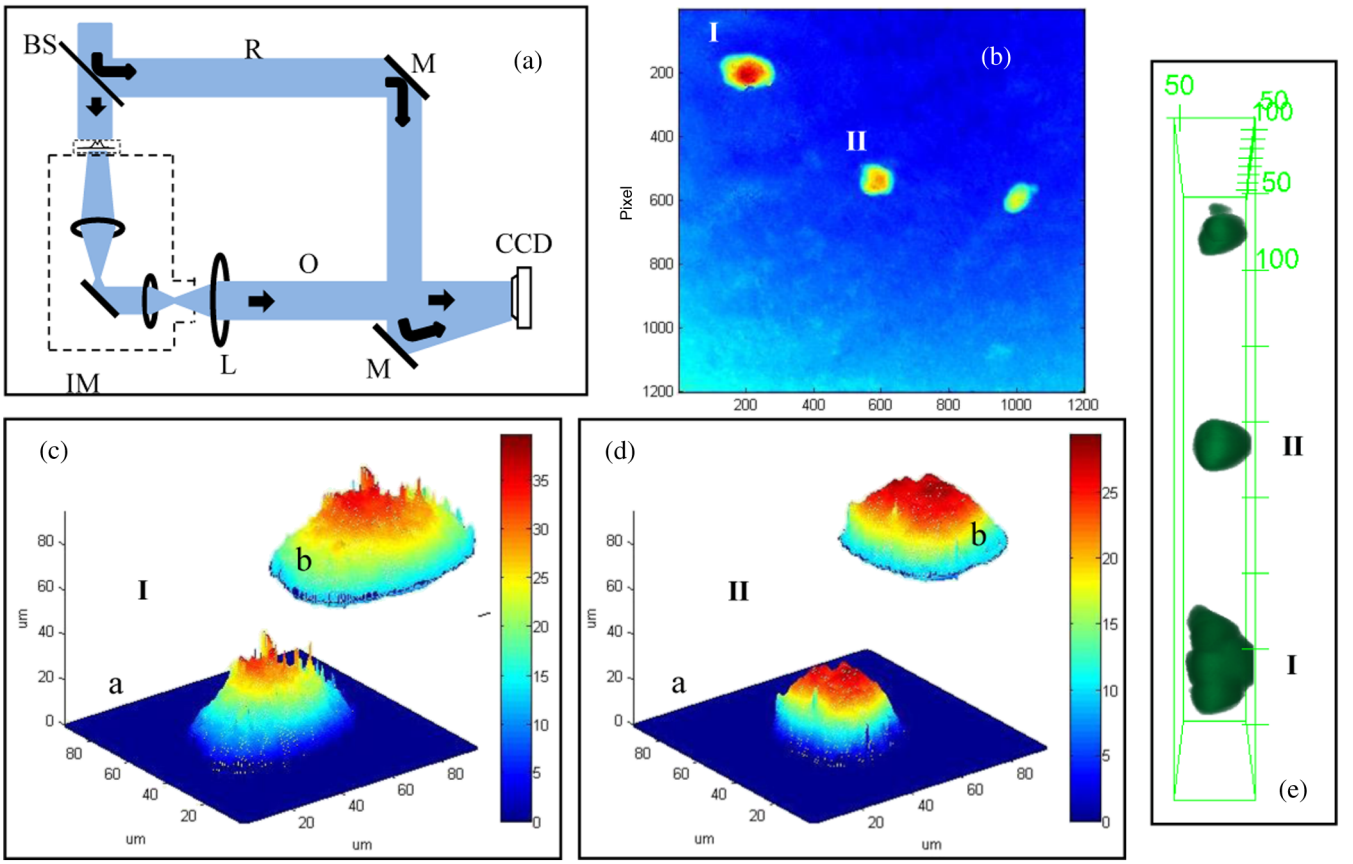

Fig. 1 (a) Schematic of the off-axis digital holographic microscopy (DHM) setup using for imaging tumor nodules. M, mirrors; BS, beam splitter; IM, inverted microscope; L, field lens; O, object beam; and R, reference beam. (b) Reconstructed unwrapped image of three-dimensional (3-D) tumor nodules. Longitudinal 3-D imaging of two nodules (I and II) are shown in panels (c) and (d). (e) Confocal images of the same nodules confirming the thickness.

as shown on day 11, where one set of oxaliplatin treatment cultures was stained with ethidium bromide (Promega Corporation, Madison, Wisconsin) and calcein (Life technologies, Oregon). For this purpose, 4-μM ethidium bromide and 2-μM calcein AM were prepared in DPBS (dulbecco's phosphate-buffered saline—balanced salt) solution obtained from HyClone Laboratories (Logan, Utah). Multichannel fluorescence images were obtained for multiple fields of each replicate of each treatment group on a Zeiss Axio Observer inverted fluorescence microscope using standard filter cubes to provide excitation of EtBr and calcein at 528 and 494 nm and the corresponding emissions were at 617 and 517 nm, respectively. Collected images were processed to estimate the total residual volume that was normalized. The total residual volume represents the sum of the volumes of individual viable nodules, while its normalized value was obtained as the ratio of total volume to that of the group and that of the no treatment control group.

3 Results and Discussion

Initially, we validated our DHM imaging system using 10 to 30-μm glass microbeads (Polysciences Inc., Warrenton, Pennsylvania) with a known index of refraction ($n_{\text{bead}} = 1.53$) that were dispersed in either water or glycerol ($n_{\text{water}} = 1.33$, $n_{\text{glyceraol}} = 1.47$). Quantitative phase measurements were used to calculate sample thickness and were compared with the object diameter in the image plane, based on the assumption of spherical geometry for glass beads. Averaging over many bead measurements, the object's diameter and thickness based on quantitative phase measurements were consistent with the object thickness within 3%.

Having validated the system on test objects, we then measured the refractive index of the tumor nodules to be used in subsequent volume calculations and treatment evaluations. As described in Sec. 2, the PANC1 3-D cultures were imaged using the holographic microscopy setup to obtain the optical path length. Figure 1(b) displays the unwrapped image of a representative cell culture that contains three nodules. Preserving the orientation, the same tumor nodules' physical thicknesses and diameters are obtained by confocal microscopy, as shown in Fig. 1(e). The unwrapped phase image is then passed through a spatial bandpass filter to improve nodule edge detection. Through a custom program, we then determined the nodule diameter, centroid, and eccentricity of each cell or nodule. The unwrapped phase measurements of individual nodules were then compared against the object height (nodule thickness) as independently measured by confocal fluorescence z-stacks to calculate a mean refractive index of 1.38, which is in agreement with the literature.[51–54] In Figs. 1(c) and 1(d), we show the longitudinal 3-D imaging of two nodules that are respectively labelled as I and II in Fig. 1(b). Figure 1(c-a) is the surface plot of cell I that is plotted on an equi-dimensional 90-μm xyz scale. The vertical color bar represents the cell thickness

in microns (obtained from unwrapped phase). The surface plot obviously does not entirely depict the actual 3-D structure. In order to generate close to a realistic 3-D plot, the surface plot is modified in such a way that one-third of the measured height of the tumor nodule was assigned as being below the center of the nodule while the remaining two-thirds were above the center. The resulting plot is shown in Fig. 1(c-b). The splitting of one-third below and two-thirds above was determined by observing confocal images of the same cell culture which is shown in Fig. 1(e). Both the surface and realistic 3-D plots show that the shapes and sizes of nodules I and II are in complete agreement with the confocal images.

3.1 *DHM Volume Analysis*

We monitored the growth of PANC-1 tumor nodules, grown for 11 days, in 3-D. Ensembles of holograms were acquired and digitally processed to obtain unwrapped phase images as described above. On day 3, cultures were assigned into groups that were treated with 20 and 100-μM oxaliplatin, in addition to

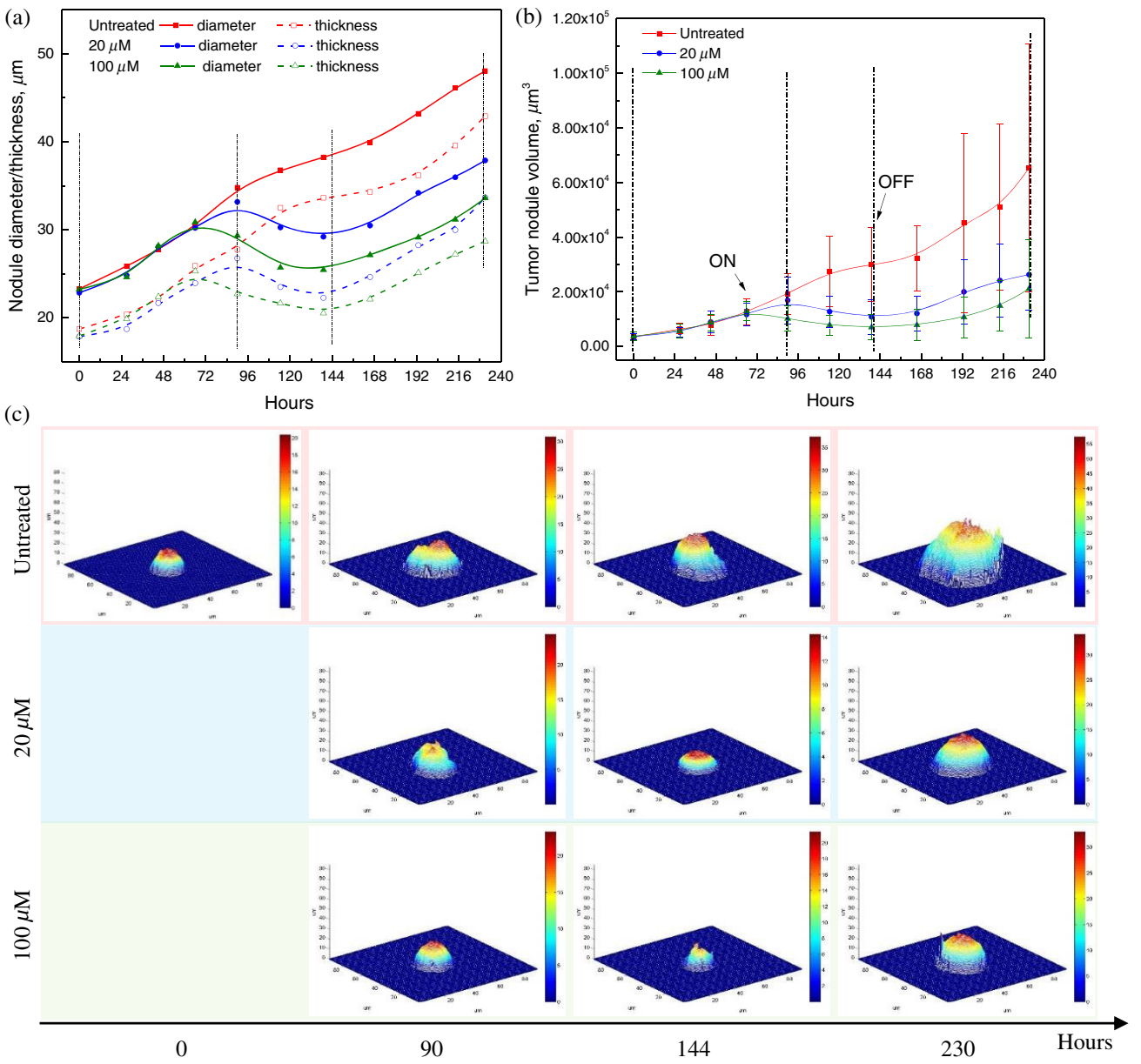

Fig. 2 DHM imaging experiments in 3-D tumor models in untreated (red) and treated (20 μM in blue and 100 μM in green) cultures using off-axis holography. (a) Plot showing the discrete time intervals at which the averaged tumor nodule diameter and thickness are obtained. The solid and dashed lines are B-spline connection between the points showing typical behavior. (b) Plot shows the variation of the tumor nodule volume where bars showing standard error are displayed on the calculated volume data points. They are omitted for clarity in (a) due to the high density of data points. (c) Representative quantitative phase reconstructions obtained from longitudinally imaging. The days at which these images are recorded are represented by vertical lines in the plots (a) and (b). The vertical color bar represents the object height in microns (obtained from unwrapped phase).

no treatment. On day 6, the oxaliplatin was removed and the tumors were allowed to grow. Figure 2(a) displays the variation of the tumor nodule diameter (solid lines) and thickness (dashed lines) averaged over reconstructions from large spatial fields containing many nodules in untreated (red) and treated (20 μM in blue and 100 μM in green) cultures. In the case of untreated samples, both the thickness and the diameter were steadily increased during the entire period of study. However, when the treatment was initiated, the tumor nodule's diameter and thickness were inhibited. The nodule size continued to decrease under the influence of oxaliplatin, but growth resumed upon removal of the cytotoxic agent as expected for regrowth following incomplete cell killing.

A provocative insight revealed in Fig. 2(b) is the delay in response to the treatment. The 100-μM treatment shows a rapid response to intervention with nodule diameter and thickness decreasing within hours of drug administration, whereas in the case of the 20-μM treatment, the tumor nodules continued growing for an additional day before decreasing in volume. Figure 2(b) represents the plot representing the average integrated 3-D volumes of PANC-1 nodules, averaged over reconstructions from large spatial fields containing many nodules in untreated (red) and treated (20 μM in blue and 100 μM in green) cultures. Bars showing the standard error, calculated from an ensemble of 60 images that were obtained per group per day, are displayed on the calculated volume data points but are omitted for clarity in Fig. 2(a) due to the high density of data points. The treatment ON and OFF time lines are indicated by arrows. It clearly displays the effect of the treatment response. As the untreated tumor nodules are steadily growing in size, the treated cultures show a decrease in the nodule volume as anticipated. Once again the noticeable difference between 20 and 100-μM cultures growth inhibition is clearly observable. In Fig. 2(c), the diameter, thickness, and corresponding volume behaviors of the tumor nodules is illustrated by phase reconstructed images. The time periods for which the representative images are selected are shown as dashed vertical lines in Figs. 2(a) and 2(b). The vertical color bar adjacent to the phase reconstructed images is the object height in microns (obtained from unwrapped phase). On the first day, Day 0, as all three groups would have similar phase-reconstructed images, only one image is shown (first column). However, for 90, 144, and 230 h (on day 4, day 5, and day 10), we show the phase reconstruction images for all three groups.

Although measurement of the cellular dry mass has also been shown to be a powerful quantitative tool by which to quantify

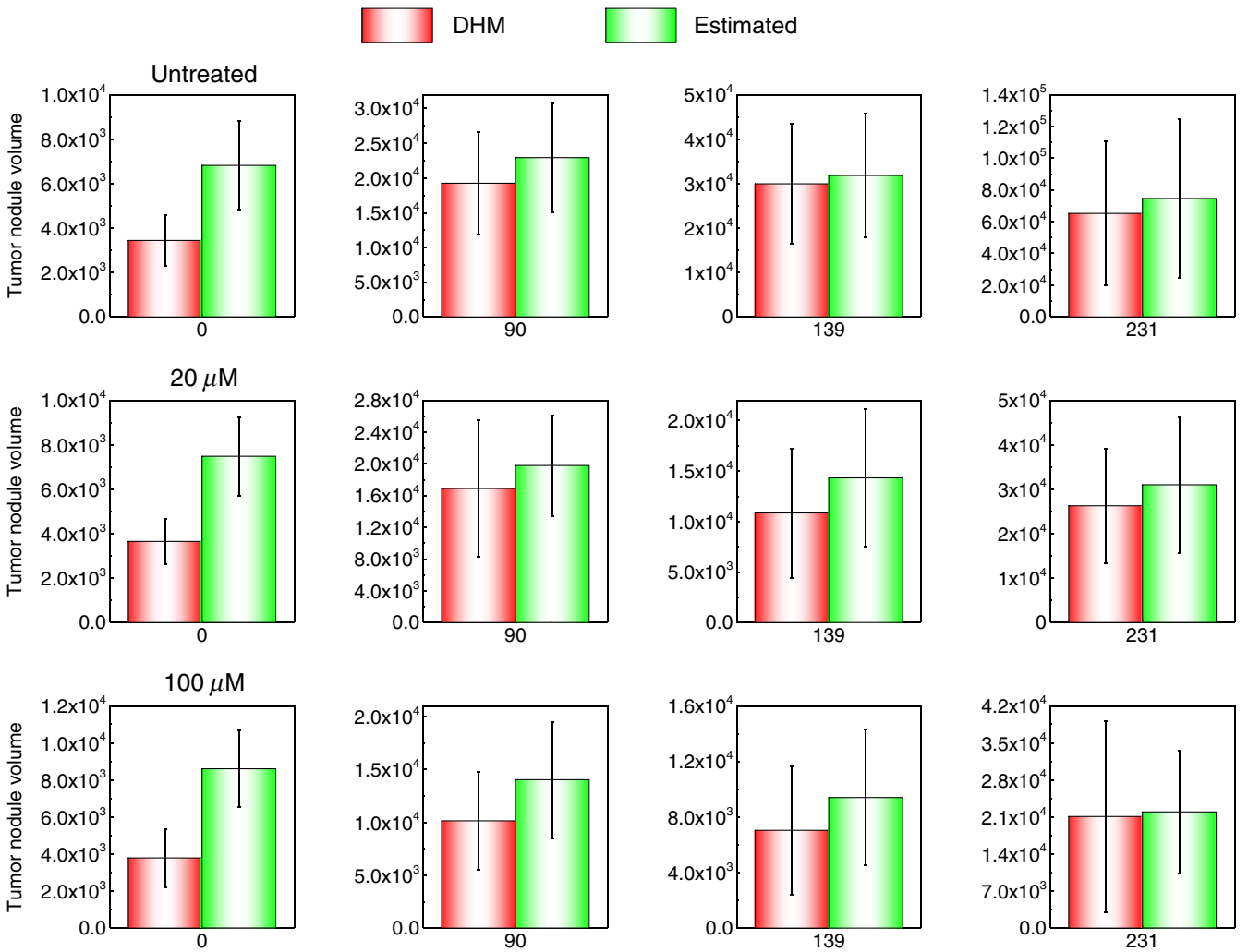

Fig. 3 Bar graph showing difference between the average integrated 3-D volumes of untreated tumor nodules obtained using DHM procedure (red) and volume estimating considering the diameter alone (green).

growth behavior,[11,12,55] the tumor volume is a more natural metric to use in this study, which is focused on monitoring therapeutic response.[56–60] Although tumor volume is a deeply established metric for treatment monitoring in clinical oncology and is widely implicated as a key prognostic indicator, it is also a logical choice for evaluation of oncology agents in preclinical systems. Although changes in the measured volume can, in fact, be driven by the osmolality of the surrounding medium in controlled experiments such as in present study, the main influence driving tumor volume change is the exposure to a cytotoxic agent which is known to reduce tumor volume by killing some fraction of the cancer cells. In addition, the current study was performed by changing the culture media at regular intervals to maintain a constant nutrient/salt balance. Therefore, while osmolality may also cause some degree of fluctuation in the measured tumor volume, the dominant effect in this treatment-focused study is due to the death of a dose-dependent fraction of the cells in each multicellular tumor nodule.

3.2 *DHM Volume and Estimated Volume Comparison*

When studying the growth rate characteristics using two-dimensional (2-D) projections obtained by qualitative phase contrast or darkfield snapshots, it is a common practice to assume the tumor nodules have a perfectly spherical geometry and only the radius is used to calculate their volumes. We termed this calculated volume as the "estimated volume." However, as the DHM images reveal 3-D information, the height of the cell is different from the radius. Therefore, the estimated volume will be different from the actual value. A bar plot comparing the tumor nodule volume to the estimated volume is shown in Fig. 3. In the untreated cultures, for the first 5 days of growth monitoring, the estimated volume is higher than that of the DHM volume. On day 6, the estimated volume is almost same as the actual volume and is lower as the days progressed. Thus, when the tumor nodule is small, the volume calculated with the assumption of spherical geometry tends to overestimate. We observed a similar trend during the treatment response period. These observations suggest that in the early stages or during the growth inhibition period, the estimated volume may lead to inaccurate growth inhibition conclusions.

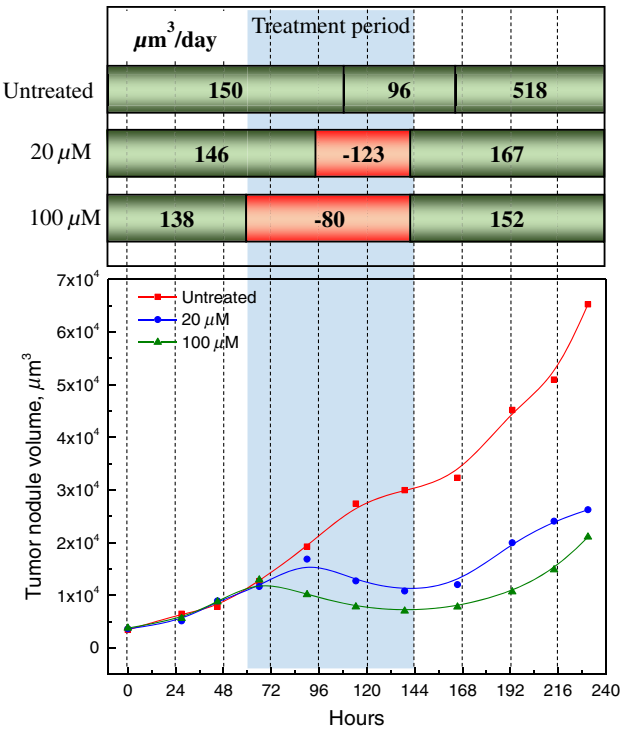

Fig. 4 Tumor nodule volume growth rate plot. Plot shows the discrete time intervals at which the averaged tumor nodule diameter was obtained. The solid lines are B-spline connection between the points showing typical behavior.

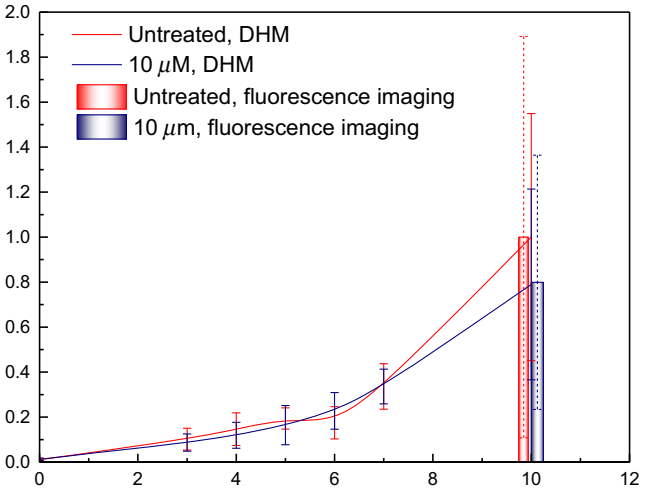

Fig. 5 Plot depicting validation of tumor volume obtained by DHM to that of the values obtained using quantification of signal from fluorescent reports of cell viability.[9]

3.3 *Volume Growth Rate Analysis*

From the tumor nodule volume plot, we calculate the volume growth rate by linear fitting various intervals. Figure 4 demonstrates the ability to quantitatively report normal and estimated growth rates and the inhibitory effect with this method. By comparison, it is evident that the 2-D imaging overestimates the growth rate, tumor inhibition, and tumor regrowth. Although the growth inhibition is delayed by a day between various dosage concentrations, their slope is the same. However, the regrowth rate for 100 μM is slight more than that for the 20 μM.

3.4 *Validation with Fluorescence Imaging*

Fractional changes in tumor volume obtained by DHM were also independently validated by an established protocol based on quantification of the signal from fluorescent reporters of cell viability,[9] as shown in Fig. 5. For this experiment, on day 8, cultures were assigned to groups that were either treated with 10-μM oxaliplatin, or received no treatment. Figure 5 shows that the longitudinal volumetric growth monitoring via DHM before and during treatment administration beside terminal quantitative fluorescence measurements from separately stained cultures are in excellent agreement.

4 Conclusion

This study demonstrates the utility of DHM as a viable approach to longitudinally and nondestructively monitor changes in the 3-D growth properties of multicellular tumor nodules. This approach, which uses relatively low-cost optical components,

is able to provide quantitative measurement of the sample depth. Using an approximate index of refraction value from the literature to convert the optical path length to sample thickness, in addition to the nodule diameter in the sample plan, we estimated the full 3-D volume of the tumor nodule. As tumor volume is the standard reporter of the disease burden, prognosis, and outcome, the ability to longitudinally measure this important parameter in a manner that would not be feasible with traditional light microscopy techniques, is significant.

Building on the reporting of overall changes in the 3-D volume described here, DHM could be further leveraged to longitudinally report the onset of important internal architectural changes such as lumen formation. With appropriately designed calibration standards, this approach can also be used to measure the mean index of refraction and this information itself could be a powerful tool in monitoring treatment response, for example in reporting contrasting optical properties of viable cells in 3-D culture and cells undergoing apoptosis. In conjunction with live cell time-lapse imaging with appropriate environmental controls, this approach could further provide 3-D holographic movies of structural development to more fully leverage these biologically-relevant models as tools to study 3-D tumor growth behavior *in vitro*. Further development and validation of the approach are warranted to correlate 3-D structural changes with signaling events evaluated by traditional terminal confocal immunofluorescence.

Acknowledgments

We gratefully acknowledge funding from the National Institutes of Health (R00CA155045, to J.P.C.) and NASA (SBIR Phase I grant NNX13CC74C, to C.S.Y.), as well as productive discussion with Dr. Imran Rizvi, of Brigham and Women's Hospital.

References

1. M. J. Bissell et al., "Tissue structure, nuclear organization, and gene expression in normal and malignant breast," *Cancer Res.* **59**(7 Suppl), 1757s–1764s (1999).
2. M. J. Bissell and D. Radisky, "Putting tumours in context," *Nat. Rev. Cancer* **1**(1), 46–54 (2001).
3. C. M. Nelson and M. J. Bissell, "Of extracellular matrix, scaffolds, and signaling: tissue architecture regulates development, homeostasis, and cancer," *Annu. Rev. Cell Dev. Biol.* **22**, 287–309 (2006).
4. J. Debnath and J. S. Brugge, "Modelling glandular epithelial cancers in three-dimensional cultures," *Nat. Rev. Cancer* **5**(9), 675–688 (2005).
5. R. Rahmanzadeh et al., "Ki-67 as a molecular target for therapy in an in vitro three-dimensional model for ovarian cancer," *Cancer Res.* **70**(22), 9234–9242 (2010).
6. I. Rizvi et al., "Synergistic enhancement of carboplatin efficacy with photodynamic therapy in a three-dimensional model for micrometastatic ovarian cancer," *Cancer Res.* **70**(22), 9319–9328 (2010).
7. L. K. Senavirathna et al., "Tumor Spheroids as an in vitro model for determining the therapeutic response to proton beam radiotherapy and thermally sensitive nanocarriers," *Theranostics* **3**(9), 687–691 (2013).
8. G. Mehta et al., "Opportunities and challenges for use of tumor spheroids as models to test drug delivery and efficacy," *J. Controlled Release* **164**(2), 192–204 (2012).
9. J. P. Celli et al., "An imaging-based platform for high-content, quantitative evaluation of therapeutic response in 3D tumour models," *Sci. Rep.* **4**, 3751 (2014).
10. J. P. Celli et al., "Quantitative imaging reveals heterogeneous growth dynamics and treatment-dependent residual tumor distributions in a three-dimensional ovarian cancer model," *J. Biomed. Opt.* **15**(5), 051603–051610 (2010).
11. G. Popescu et al., "Optical imaging of cell mass and growth dynamics," *Am. J. Physiol.-Cell Physiol.* **295**(2), C538–C544 (2008).
12. B. Rappaz et al., "Noninvasive characterization of the fission yeast cell cycle by monitoring dry mass with digital holographic microscopy," *J. Biomed. Opt.* **14**(3), 034049 (2009).
13. G. Popescu, *Quantitative Phase Imaging of Cells and Tissues*, McGraw-Hill Education, New York (2011).
14. M. Mir et al., "Quantitative phase imaging," *Progr. Opt.: Elsevier Sci. Ltd.* **57**(July), 133–217 (2012).
15. M. Mir et al., "Highly sensitive quantitative imaging for monitoring single cancer cell growth kinetics and drug response," *PloS One* **9**(2), e89000 (2014).
16. M. K. Kim, "Digital Holographic Microscopy," in *Digital Holographic Microscopy*, pp. 149–190, Springer (2011).
17. B. Kemper et al., "Digital holographic microscopy: quantitative phase imaging and applications in live cell analysis," *Handbook of Coherent-Domain Optical Methods*, Vol. 1, p. 215, Springer Science+ Business Media, New York (2013). ISBN 978–1-4614-5175-4
18. E. Cuche, P. Marquet, and C. Depeursinge, "Simultaneous amplitude-contrast and quantitative phase-contrast microscopy by numerical reconstruction of Fresnel off-axis holograms," *Appl. Opt.* **38**(34), 6994–7001 (1999).
19. P. Marquet et al., "Digital holographic microscopy: a noninvasive contrast imaging technique allowing quantitative visualization of living cells with subwavelength axial accuracy," *Opt. Lett.* **30**(5), 468–470 (2005).
20. F. Charriere et al., "Cell refractive index tomography by digital holographic microscopy," *Opt. Lett.* **31**(2), 178–180 (2006).
21. B. Das and C. S. Yelleswarapu, "Dual plane in-line digital holographic microscopy," *Opt. Lett.* **35**(20), 3426–3428 (2010).
22. L. Yu et al., "Digital holographic microscopy for quantitative cell dynamic evaluation during laser microsurgery," *Opt. Express* **17**(14), 12031–12038 (2009).
23. B. Rappaz et al., "Measurement of the integral refractive index and dynamic cell morphometry of living cells with digital holographic microscopy," *Opt. Express* **13**(23), 9361–9373 (2005).
24. P. Memmolo et al., "Investigation on 3D morphological changes of in vitro cells through digital holographic microscopy," *SPIE Opt. Metrol.* **8792**, 87920R (2013).
25. J. Kühn et al., "Label-free cytotoxicity screening assay by digital holographic microscopy," *Assay Drug Dev. Technol.* **11**(2), 101–107 (2013).
26. K. Badizadegan et al., "Speckle-field digital holographic microscopy," *Opt. Express* **17**(15), 12285–12292 (2009).
27. P. Gao, G. Pedrini, and W. Osten, "Structured illumination for resolution enhancement and autofocusing in digital holographic microscopy," *Opt. Lett.* **38**(8), 1328–1330 (2013).
28. I. Yamaguchi et al., "Image formation in phase-shifting digital holography and applications to microscopy," *Appl. Opt.* **40**(34), 6177–6186 (2001).
29. X. F. Meng et al., "Two-step phase-shifting interferometry and its application in image encryption," *Opt. Lett.* **31**(10), 1414–1416 (2006).
30. J. P. Liu and T. C. Poon, "Two-step-only quadrature phase-shifting digital holography," *Opt. Lett.* **34**(3), 250–252 (2009).
31. N. T. Shaked, M. T. Rinehart, and A. Wax, "Dual-interference-channel quantitative-phase microscopy of live cell dynamics," *Opt. Lett.* **34**(6), 767–769 (2009).
32. N. T. Shaked et al., "Two-step-only phase-shifting interferometry with optimized detector bandwidth for microscopy of live cells," *Opt. Express* **17**(18), 15585–15591 (2009).
33. N. T. Shaked et al., "Parallel on-axis holographic phase microscopy of biological cells and unicellular microorganism dynamics," *Appl. Opt.* **49**(15), 2872–2878 (2010).
34. B. Das, C. S. Yelleswarapu, and D. Rao, "Parallel-quadrature phase-shifting digital holographic microscopy using polarization beam splitter," *Opt. Commun.* **285**(24), 4954–5960 (2012).
35. C. L. Evans et al., "Visualizing photodynamic therapy response with time-lapse OCT in an *in vitro* model of metastatic ovarian cancer," *Proc. SPIE* **7551**, 75510J (2010).
36. C. L. Evans et al., "In vitro ovarian tumor growth and treatment response dynamics visualized with time-lapse OCT imaging," *Opt. Express* **17**(11), 8892–8906 (2009).
37. P. Bon et al., "Optical detection and measurement of living cell morphometric features with single-shot quantitative phase microscopy," *J. Biomed. Opt.* **17**(7), 076004 (2012).
38. N. T. Shaked, "Quantitative phase microscopy of biological samples using a portable interferometer," *Opt. Lett.* **37**(11), 2016–2018 (2012).

39. Y. Choi et al., "Full-field and single-shot quantitative phase microscopy using dynamic speckle illumination," *Opt. Lett.* **36**(13), 2465–2467 (2011).
40. P. Bon et al., "Quadriwave lateral shearing interferometry for quantitative phase microscopy of living cells," *Opt. Express* **17**(15), 13080–13094 (2009).
41. N. Lue et al., "Quantitative phase imaging of live cells using fast Fourier phase microscopy," *Appl. Opt.* **46**(10), 1836–1842 (2007).
42. M. G. L. Gustafsson, "Surpassing the lateral resolution limit by a factor of two using structured illumination microscopy," *J. Microsc.-Oxford* **198**(2), 82–87 (2000).
43. L. Shao et al., "Super-resolution 3D microscopy of live whole cells using structured illumination," *Nat. Methods* **8**(12), 1044–1046 (2011).
44. F. Dubois et al., "Digital holographic microscopy for the three-dimensional dynamic analysis of in vitro cancer cell migration," *J. Biomed. Opt.* **11**(5), 054032 (2006).
45. P. Langehanenberg et al., "Automated three-dimensional tracking of living cells by digital holographic microscopy," *J. Biomed. Opt.* **14**(1), 014018 (2009).
46. A. Kuś et al., "Tomographic phase microscopy of living three-dimensional cell cultures," *J. Biomed. Opt.* **19**(4), 046009 (2014).
47. M. D. Glidden et al., "Image-based quantification of benzoporphyrin derivative uptake, localization, and photobleaching in 3D tumor models, for optimization of PDT parameters," *Theranostics* **2**(9), 827–839 (2012).
48. G. Y. Lee et al., "Three-dimensional culture models of normal and malignant breast epithelial cells," *Nat. Methods* **4**(4), 359–365 (2007).
49. C. Mann et al., "High-resolution quantitative phase-contrast microscopy by digital holography," *Opt. Express* **13**(22), 8693–8698 (2005).
50. E. Cuche, F. Bevilacqua, and C. Depeursinge, "Digital holography for quantitative phase-contrast imaging," *Opt. Lett.* **24**(5), 291–293 (1999).
51. W. J. Choi et al., "Full-field optical coherence microscopy for identifying live cancer cells by quantitative measurement of refractive index distribution," *Opt. Express* **18**(22), 23285–23295 (2010).
52. A. Khmaladze et al., "Cell volume changes during apoptosis monitored in real time using digital holographic microscopy," *J. Struct. Biol.* **178**(3), 270–278 (2012).
53. B. Kemper et al., "Investigation of living pancreas tumor cells by digital holographic microscopy," *J. Biomed. Opt.* **11**(3), 034005 (2006).
54. M. Kemmler et al., "Noninvasive time-dependent cytometry monitoring by digital holography," *J. Biomed. Opt.* **12**(6), 064002 (2007).
55. S. Sridharan, M. Mir, and G. Popescu, "Simultaneous optical measurements of cell motility and growth," *Biomed. Opt. Express* **2**(10), 2815–2820 (2011).
56. V. Göbel et al., "Prognostic significance of tumor volume in localized Ewing's sarcoma of bone in children and adolescents," *J. Cancer Res. Clin. Oncol.* **113**(2), 187–191 (1987).
57. J. D. Bradley et al., "Gross tumor volume, critical prognostic factor in patients treated with three-dimensional conformal radiation therapy for non-small-cell lung carcinoma," *Int. J. Radiat. Oncol. Biol. Phys.* **52**(1), 49–57 (2002).
58. T. R. Miller and P. W. Grigsby, "Measurement of tumor volume by PET to evaluate prognosis in patients with advanced cervical cancer treated by radiation therapy," *Int. J. Radiat. Oncol. Biol. Phys.* **53**(2), 353–359 (2002).
59. J. Epstein et al., "Is tumor volume an independent predictor of progression following radical prostatectomy? A multivariate analysis of 185 clinical stage B adenocarcinomas of the prostate with 5 years of followup," *J. Urol.* **149**(6), 1478–1481 (1993).
60. R. J. Geer and M. F. Brennan, "Prognostic indicators for survival after resection of pancreatic adenocarcinoma," *Am. J. Surg.* **165**(1), 68–73 (1993).

Yuyu Li is a PhD student at Boston University. He received his MS in applied physics in May 2014 from the University of Massachusetts Boston. He worked in Yelleswarapu's lab for his master's thesis project.

Ljubica Petrovic is a PhD student at BMEBT at the University of Massachusetts in Boston. At the same time she works in Celli lab on her PhD thesis. She received her MS from the same university in the Applied Physics Program in 2013.

Jefrrey La is a MS student in the Applied Physics Program at the University of Massachusetts in Boston. He is working in Yelleswarapu's lab on his MS thesis project. He received a bachelor's degree in physics from the same university in May 2014.

Jonathan P. Celli is an assistant professor in the Department of Physics at the University of Massachusetts in Boston, Massachusetts. Previously he was an instructor at the Wellman Center for Photomedicine at Massachusetts General Hospital, where he also received his postdoctoral training. The Celli lab conducts research in cancer biophysics, biomedical imaging, and photomedicine.

Chandra S. Yelleswarapu is an assistant professor in the Department of Physics at the University of Massachusetts in Boston, Massachusetts. He received his postdoctoral training at the University of New Mexico, Albuquerque, and the University of Massachusetts Boston. Yelleswarapu's lab conducts research in the areas of phase imaging, nonlinear optics, photoacoustics, and biomedical imaging.